Journal of
Manufacturing and Materials Processing

MDPI

Communication

Investigation of the Shape and Detectability of Pores with X-ray Computed Tomography

Benjamin Baumgärtner [1,2,3,*], Juan Hussein [1,2] and Tino Hausotte [1,2,3]

[1] Department of Mechanical Engineering, Faculty of Engineering, Friedrich-Alexander-Universität Erlangen-Nürnberg (FAU), Schloßplatz 4, 91054 Erlangen, Germany
[2] Collaborative Research Center 814—Additive Manufacturing (CRC 814), Am Weichselgarten 10, 91058 Erlangen, Germany
[3] Institute of Manufacturing Metrology (FMT), Nägelsbachstr. 25, 91052 Erlangen, Germany
* Correspondence: benjamin.baumgaertner@fmt.fau.de; Tel.: +49-9131-85-20452

Abstract: Component porosity is a quality attribute in additive manufacturing (AM). One possibility for the non-destructive three-dimensional determination of porosity or pore shape is X-ray computed tomography (CT), which enables an investigation of the influence of AM process parameters on the appearance and characteristics of the pores. Since there is no porosity standard for CT, a traceable determination of the measurement uncertainty is not possible. Using a digital twin of the CT system, an estimation of the CT measurement uncertainty is in principle possible. In this contribution, experimental CT analyses of powder bed fusion samples made of Ti64 and PA12 are compared with CT simulations. The results show a size-dependent influence on the shape and detectability of the pores. Using the CT model, a simulated shape- and material-dependent probability of detection (POD) is calculated.

Keywords: computed tomography; porosity measurement; additive manufacturing; Ti64; PA12

Citation: Baumgärtner, B.; Hussein, J.; Hausotte, T. Investigation of the Shape and Detectability of Pores with X-ray Computed Tomography. *J. Manuf. Mater. Process.* **2023**, *7*, 103. https://doi.org/10.3390/jmmp7030103

Academic Editors: Dietmar Drummer, Michael Schmidt and David Bourell

Received: 6 April 2023
Revised: 12 May 2023
Accepted: 21 May 2023
Published: 23 May 2023

1. Introduction

Additive manufacturing (AM) offers the potential to produce highly complex geometric parts at a fraction of the usual cost [1]. Nevertheless, the process-related low surface quality [2] and the limitation of the achievable density, e.g., in laser-based powder bed fusion of metals (LB-PBF/M), compared to forging and casting [3] are among the main reasons why it is difficult finding commercial applications for AM parts. Component density represents a quality characteristic of the manufacturing process and is therefore more in focus. The main source of internal defects such as pores or channels is the temperature profile and process-related parameters such as beam power, hatch distance, and layer thickness. Commonly used micrograph imaging allows the evaluation of the shape, size, position, and classification of defects in 2D [4]. However, this technique has difficulties in detecting defects near edges and along the fabrication direction [5]. X-ray computed tomography (CT) is a practical way for a three-dimensional, non-destructive measurement in a single post-process measurement [6,7]. From the gray value volume data as output of the CT scan, the transition from material to background has to be defined by surface determination [8,9]. According to [10], a globally determined gray value for the outer surface contour, however, cannot be used to properly detect the material transition of inner defects such as pores. The use of a surface determination procedure for the evaluation of the geometric properties of defects can lead to errors, as there is a mismatch between the gray value level of the defects and the gray value level of the background and thus a wrongly assumed threshold for the transition. A classification of the pores depending on the process parameters used, as described by Snell et al. [4], would be a useful tool when transferred to CT analysis. However, a transfer of the classification can only be successful if the measurement uncertainty of the CT porosity analysis is calculated. Due to the lack

of porosity standards for CT, the use of CT simulation is a potential option to estimate a measurement uncertainty for porosity analysis. For this research, a CT simulation with an adapted CT model of a real CT measuring system is used. In the CT simulation, a computer-aided design (CAD) model of an AM sample with incorporated process-related pores is used to determine measurement deviations for the pore shape and a probability of detection (POD) to estimate the detection limit. The simulation results are compared with experimental CT measurements of samples made of the titanium alloy Ti-6Al-4V (Ti64) and samples made of polymer polyamide (PA12).

2. Materials and Methods

2.1. Samples

The sample geometry has a cylindrical shape following the recommendations of ASTM 1570.11 [11]. The rotational symmetry leads to constant X-ray transmission lengths during the CT measurement, which has a beneficial effect regarding CT imaging artifacts. The specimen has a height of 8.7 mm (measured without reference and support structures) and a diameter of 5 mm. The manufacturing parameters for the two specimens are shown in Table 1. In order to reference the position of the detected defects in relation to the sample geometry, one-quarter of the cylinder with a height of 1 mm is left free at the top as shown in Figure 1. This structure is used to align the coordinate system and to define regions of interest (ROI) around observed pores for POD analysis.

Table 1. Process parameters of the LB-PBF/M for the Ti64 samples and the LB-PBF/P for the PA12 sample.

	Unit	PBF/M	PBF/P
Material		Ti64	PA12
Machine		Aconity Mini	Research System
Beam power	W	900	16
Beam diameter	µm	90	500
Scanning speed	mm s^{-1}	1200	2000
Hatch line spacing	µm	120	200
Layer thickness	µm	50	100

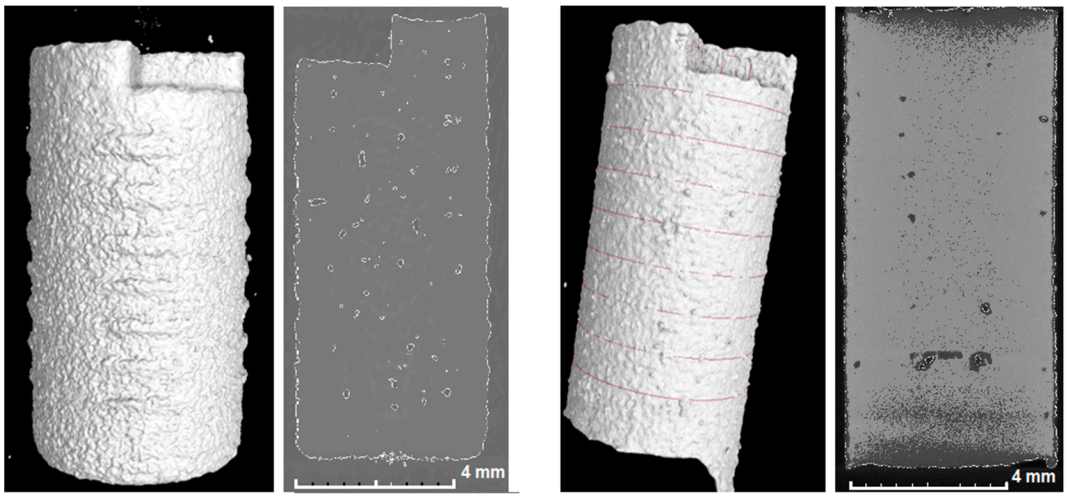

(**a**) (**b**)

Figure 1. The 3D CT image of the samples of (**a**) PA12 and (**b**) Ti64.

2.2. CT Measurement

A Metrotom 1500 industrial X-ray computed tomograph (Carl Zeiss AG, Oberkochen Germany) was used for the CT measurements of both samples. The detector has a size

of 2048 × 2048 pixel, with a pitch of 0.2 mm. The detector settings include gain: 16×, integration time: 2000 ms, frame averaging: off/10× (for PA12). A copper prefilter with a thickness of 0.5 mm was used. The samples were rotated by 360° in 0.2° increments, corresponding to 1800 projected images. Due to the material-specific absorption contrast, the X-ray tube parameters are different for PA12 and Ti64. A voltage of 140 kV and a current of 150 µA were used for PA12 and 190 kV and 70 µA for Ti64. This results in a native voxel size (vx) of 8 µm and 7.32 µm related to a magnification of 28 and a focal spot size (fs) of 22 µm and 13 µm, respectively. Please note that the CT parameters used are specific to the system used and cannot be directly transferred to other CT systems. The choice of parameter sets refers to [12] and [13]. Images are stored in the raw data format (uint16 encoding) and reconstructed using the Feldkamp–Davis–Kress (FDK) reconstruction algorithm with a Shepp–Logan filter [14].

2.3. CT Simulation

The CT simulation is performed using the software BAM aRtist 2.10 (Bundesanstalt für Materialforschung und -prüfung BAM, Berlin Germany) and a simulation model of the X-ray source and detector that is adapted to the real CT system. The parametrization for source and detector are reasonably approximated to the parameters as described in 2.3 with a simulated shot noise. The sample model combines the CAD template from the manufacturing process with CAD models of pores extracted from micrographs, shown in Figure 2. The pores vary in sphericity from 100% for an ideal sphere to 20% for lack-of-fusion pores as determined by the equation shown in Equation (1). Here, A_{sphere} corresponds to the area of an ideal sphere with the same volume as the detected defect and is related to the area $A_{detected}$ of the defect. Since, in principle, different pore shapes can lead to the same sphericity value, the compactness C (Equation (2)) was also considered for the design of the pore models. The compactness sets the detected volume $V_{detected}$ in relation to the volume $V_{envelope}$ of an enveloping sphere around this defect. Using suitable models, a compactness variation from 10% to 30% was implemented for pores with a sphericity ranging from 40% to 60%. To determine the POD, the pores must vary in size to pass the detection limit. Therefore, the pore models are scaled homogenously.

$$\psi = A_{sphere} / A_{detected} \quad (1)$$

$$C = V_{detected} / V_{envelope} \quad (2)$$

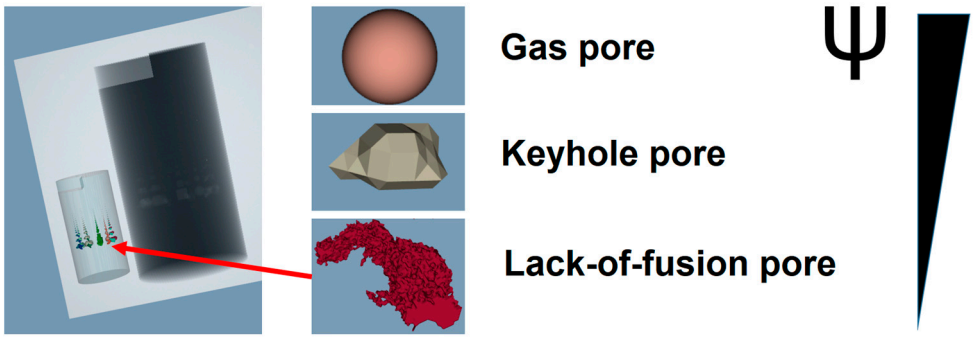

Figure 2. CT simulation in the software aRTist with CAD pore models.

2.4. Metrological Evaluation

The metrological processing of gray value-based volume data is performed using the software VGStudio Max Version 2022.2 (Volume Graphics GmbH, Heidelberg Germany). First, for PA12, a non-local-means filtering [15] of the voxel dataset is applied to reduce noise with a smoothing factor of 1.8. Then, the outer surface of the sample is determined using the advanced (classic) approach with the iterative determination option enabled. The

porosity analysis is performed using the VGDefX algorithm with the "Only-Threshold" option. The material definition is set to "use surface determination" and the deviation of the gray value threshold for the maximum pore gray value is defined according to the BDG P203 guideline [16]. The probability criterion is set to 0 and the minimum pore size filter is set to 1 vx. The output of the algorithm includes the size, shape (e.g., the sphericity), and position of each pore within the volume.

2.5. Calculation of the Probability of Detection

The POD is calculated manually by observing the pore position within 20 repeat measurements for the CT measurements and for the CT simulation by using the CAD template. The template is aligned with the reference structure on top and a ROI is drawn with a 10 vx spacing in each direction and placed around the expected position of the pore. The porosity algorithm is then run and the results are observed and filtered. If more than one pore is detected, a size-dependent filtering is performed, which always takes the pore with a size more similar to the reference for the CT simulation. For the CT measurements, an initial "reference" measurement is performed and used as "ground truth" with a frame to average of 20 and an integration time of 2000 ms to reduce statistical influences. Due to the large number of detectable pores, the observation is limited to 100 pores of different size (3–50 vx) and shape.

2.6. Synchrotron CT Measurement

In order to better assess the influence of noise and CT-dependent artifacts, comparison measurements were carried out on parts of the two samples with a volume of 1 mm^3 using the snychrotron CT Bamline (BAM). A voxel size of 1 µm was achieved for Ti64 and PA12. The porosity analysis has been performed with the same options mentioned in 2.5. Please note that in order to compare the CT and the synchrotron CT measurements in terms of the shape recognition, the pore size is normalized to voxel size and the actual size of the pores is not compared.

3. Results

Performing a CT simulation with the adapted CT model and process-related pore models and assuming an ideal shape detectability, all pores would be detected with the insert sphericity values up to the detection limit. Figure 3a shows the sphericity of the pores in the Ti64 sample (reference measurement) for CT measurement (blue circles) and for CT simulation (colored solid lines with error bars). From the simulation results, it can be derived that there is a large systematic (negative) offset for the measured sphericity values with regard to the true values. For example, for ideally spherical gas pores, values of approximately 60% are obtained instead of 100%. As values between 20% and 60% are typically dedicated to lack of fusion, the systematic error would lead to a wrong classification. Without knowledge about how the CT characteristics change the values, most of the found pores (for simulation as well as experiment) would be classified as lack-of-fusion pores. In addition to the offset, as the pore size decreases below 25 vx, the measured sphericity increases and a portion of the pores would be classified as keyhole pores (ψ: (70 to 80)%) if the classification from micrographs [4] is applied directly (red, yellow and green lines). In general, with a decreasing pore diameter, an increase in the measured pore sphericity can be observed, which affects lack-of-fusion pores more than the gas or keyholes pores. A rounding effect is assumed as cause for this.

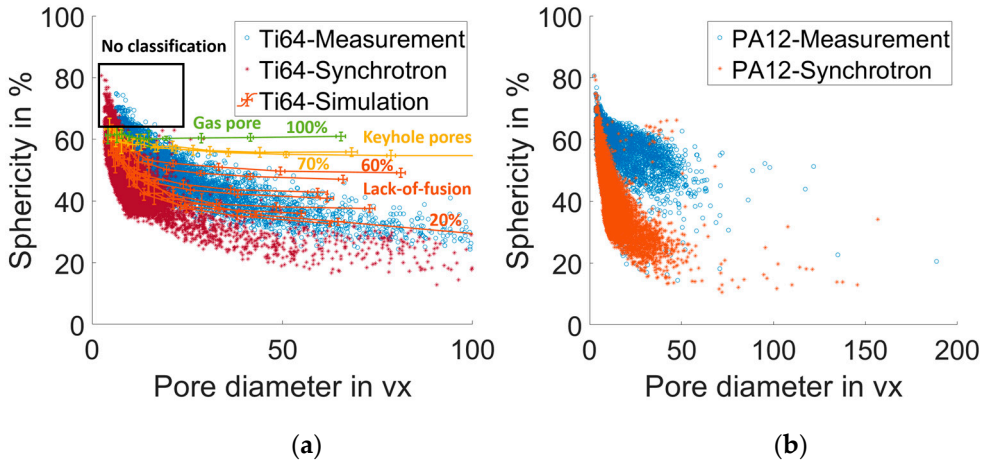

Figure 3. Sphericity of pores in (**a**) Ti64 and (**b**) in PA12 for the CT measurement (blue asterisk), the synchrotron CT measurement (red/orange asterisk), and colored solid line with error bars for the CT simulation.

As the pore diameter increases, the sphericity of gas and keyhole pores become more constant in the simulation, while the measured sphericity of lack-of-fusion pores decreases significantly. Furthermore, pores with higher sphericity than the one that would be expected for gas pores occur in the CT simulation but are not due to inserted pores. Since there is a possibility of false detections due to noise of the material gray values and due to CT artifacts, this classification needs to be supplemented in relation to [4] when transferred to the CT analyze. The CT measurement for Ti64 (blue asterisk) show a very similar behavior when compared to the CT simulation. It is worth noting that pores below the lowest recorded pore shape appear in the real measurement. Considering that low spherical pores also show lower sphericity in CT analysis, it can be assumed that the pores are in the range of (0 to 20)% sphericity, which are not included in the CT simulation model. Figure 3b shows the same analysis for PA12. Unfortunately, the CT simulation cannot reproduce the material contrast very well and a porosity analysis fails due to high noise.

Figure 4a shows the respective PODs of the CT simulation for Ti64 (a) as solid lines and the data points (blue) of the CT measurements. Since this study examines detectability in terms of pore shape (sphericity), but pore can have a different compactness values while the sphericity remains constant, the calculated CT POD are plotted as single measurement points and nor as usually as solid lines. As expected, there is a pore shape-dependent effect on the POD and hence a shape-dependent detection limit. As the sphericity increases, the detection limit shifts to smaller pore diameters and the step of the function becomes sharper, as seen for gas (green) and keyhole pores (yellow). For the quite large range of lack-of-fusion pores, the step function becomes flatter. The calculated POD of the CT measurement Figure 4a (blue) covers the results of the CT simulation very well. Figure 4b shows the comparative measurement of the PA12 CT measurement (blue asterisk).

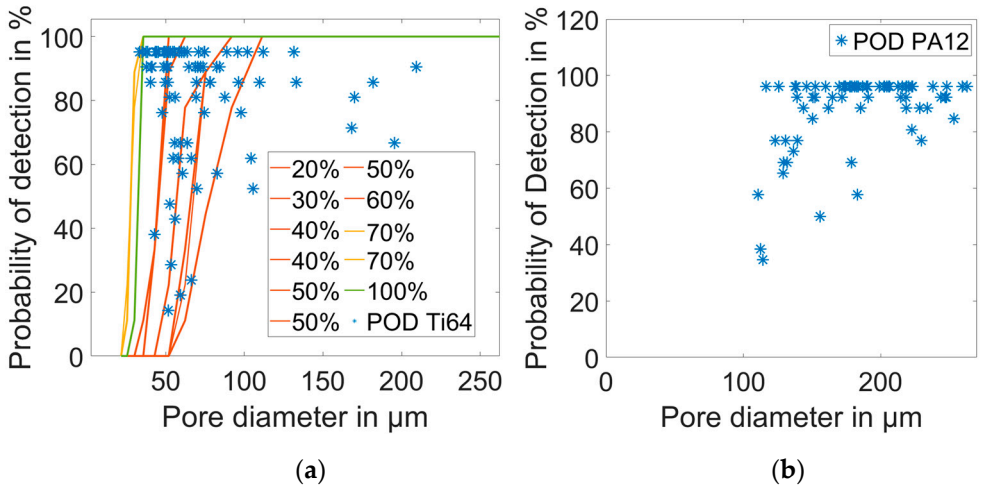

Figure 4. Probability of detection of pores in (**a**) Ti64 for the real measurement (blue asterisk), lack of fusion (20 to 60)%, keyholes 70%, and gas pores 100% for CT simulation (colored solid line) and (**b**) PA12 for CT measurements (blue asterisk).

4. Discussion

First of all, it should be noted that the influence of CT on pore shape detection is not traceable in the absence of a porosity standard. However, according to the definition of the sphericity in Equation (1), the sphericity increases as the surface of the analyzed pore becomes more similar to the surface of an ideal sphere. Since ideal spheres in the CT simulation did not reach values higher than 60%, there has to be an increase in the detected surfaces, within constant pore size. It is assumed that there are two main reasons for this. The first reason is noise, which affects the gray data and can lead to local deviation, which leads to a rough surface when using global thresholds for the determination. This influence is statistical but affects all pores in more or less the same way, which may explain the constant offset of the gas pores in the CT simulation data. The second reason a rounding effect that scales with pore size. A comparison of the CT with the synchrotron CT measurement in Figure 3 shows that the measured pore sphericity occurring in the components is significantly smaller for synchrotron CT, but a rounding effect can also be observed. This affects smaller pores more than larger ones, as can be seen in Figure 4a for the lack of fusion, but does not affect the gas pores. Since synchrotron CT has a higher resolution, lower noise and fewer CT artifacts and can be used as a reference, it is assumed that noise, resolution and artifacts for pores with many edges will have a smoothing effect on the surface when compared to µ-CT measurements. In contrast, gas pores behave consistently with respect to the sphericity, and it is assumed that the influence of the rounding effect does not smooth the surface of gas pores. In summary, the increased surface area due to noise does not change the macroscopic shape of the pores, which leads to a misclassification of, e.g., gas pores and, at least within the CT simulation, the sphericity remains constant over the scaling pore size. The rounding effect, which changes the macroscopic shape of the pore when scaling the pore size, smooths corners and edges in the example of lack-of-fusion pores and leads to an increase in sphericity for angular pores. On the other hand, keyholes and gas pores, which are highly spherical, are almost unaffected.

In addition to the rounding effect and sphericity offset in the CT simulation, the POD is affected, as highly spherical pores reach a lower detection limit. Assuming that gas pores occur with 60% sphericity and that this is the upper limit of the lack-of-fusion range, this pore category should achieve significantly higher detectability. This analysis shows that even pores with diameters that are significantly larger than the default value of 3 voxel diameter limit in the porosity analyses can have PODs different from 100%, even for pores with 10 vx and larger diameters. In order to correctly assess the POD of a pore, the sphericity must be completely traced back.

5. Conclusions

In summary, the influences on the pore shape in CT analysis are too strong to transfer a direct Snell classification from micrographs, as gas and keyhole pores would not be correctly recognized. Since the sphericity criterion seems to be too sensitive to noise and CT artifacts, and thus even highly spherical pores would not be classified correctly, the definition should be adapted accordingly. However, as the influence of CT systems may vary, a direct normalization of the maximum sphericity achieved by gas pores does not make sense. A suggestion at least for gas pores is to evaluate the shape deviation from a Gaussian sphere. Since for all other pores no reference geometry is available, the evaluation of the pores by comparison with a sphere probably remains the best possibility. Although the CT simulation shows good agreement with the real CT measurements and a shape-dependent POD can be derived, among the main criticisms of this study is the transfer of the simulation results to the real measurement. However, the inserted pores in the CT simulation show a reduction in sphericity, and the sphericity of the pore in the CT measurement shows an increase when compared with the results of the synchrotron CT measurement. Nevertheless, this shows the need for a pore standard for CT analysis.

Author Contributions: Conceptualization, B.B.; methodology, B.B.; software, B.B., J.H.; validation, B.B and T.H.; formal analysis, B.B.; investigation, B.B.; resources, B.B.; data curation, B. Baumgärtner.; writing—original draft preparation, B.B.; writing—review and editing, T.H.; visualization, B.B. and J.H.; supervision, T.H.; project administration, T.H.; funding acquisition, T.H. All authors have read and agreed to the published version of the manuscript.

Funding: This study has been funded by the Deutsche Forschungsgemeinschaft (DFG, German Research Foundation)—Project-ID 61375930–SFB814, Subproject C4. The financial support is gratefully acknowledged.

Data Availability Statement: The data presented in this study are available on request from the corresponding author.

Conflicts of Interest: The authors declare no conflict of interest.

References

1. Brückner, F.; Leyens, C. Hybrid laser manufacturing. In *Laser Additive Manufacturing*; Elsevier: Amsterdam, The Netherlands, 2017; pp. 79–97.
2. Gockel, J.; Sheridan, L.; Koerper, B.; Whip, B. The influence of additive manufacturing processing parameters on surface roughness and fatigue life. *Int. J. Fatigue* **2019**, *124*, 380–388. [CrossRef]
3. Dutta, B.; Froes, F.H.S. The additive manufacturing (AM) of titanium alloys. *Met. Powder Rep.* **2017**, *72*, 96–106. [CrossRef]
4. Snell, R.; Tammas-Williams, S.; Chechik, L.; Lyle, A.; Hernández-Nava, E.; Boig, C.; Panoutsos, G.; Todd, I. Methods for Rapid Pore Classification in Metal Additive Manufacturing. *JOM* **2020**, *72*, 101–109. [CrossRef]
5. Liu, X.; Chu, P.K.; Ding, C. Surface modification of titanium, titanium alloys, and related materials for biomedical applications. *Mater. Sci. Eng. R Rep.* **2004**, *47*, 49–121. [CrossRef]
6. Pavan, M.; Craeghs, T.; Verhelst, R.; Ducatteeuw, O.; Kruth, J.-P.; Dewulf, W. CT-based quality control of Laser Sintering of Polymers. *Case Stud. Nondestruct. Test. Eval.* **2016**, *6*, 62–68. [CrossRef]
7. Wingham, J.R.; Turner, R.; Shepherd, J.; Majewski, C. Micro-CT for analysis of laser sintered micro-composites. *Rapid Prototyp. J.* **2020**, *26*, 649–657. [CrossRef]
8. Kittler, J.; Illingworth, J. Illingworth. Minimum Error Thresholding. *Pattern Recognit.* **1986**, *19*, 41–47. [CrossRef]
9. Otsu, N. A Threshold Selection Method from Gray-Level Histograms. *IEEE Trans. Syst. Man Cybern.* **1979**, *9*, 62–66. [CrossRef]
10. Jaques, V.A.J.; Du Plessis, A.; Zemek, M.; Šalplachta, J.; Stubianová, Z.; Zikmund, T.; Kaiser, J. Review of porosity uncertainty estimation methods in computed tomography dataset. *Meas. Sci. Technol.* **2021**, *32*, 122001. [CrossRef]
11. *ASTM E1570-11*; 1570-11-Standard Practice for Computed Tomographic (CT) Examination. ASTM International, United States: West Conshohocken, PA, USA, 2011.
12. Bellens, S.; Vandewalle, P.; Dewulf, W. Deep learning based porosity segmentation in X-ray CT measurements of polymer additive manufacturing parts. *Procedia CIRP* **2021**, *96*, 336–341. [CrossRef]
13. ZEISS. ZEISS CT Cookbook-English Edition: Best Practice Guide for ZEISS METROTOM Settings, Germany. Available online: https://shop.metrology.zeiss.de/INTERSHOP/web/WFS/IMT-DE-Site/de_DE/-/EUR/ViewProduct-Start?SKU=600033-2022-016&CategoryName=240100&CatalogID=200000&ExtendedNavigation=true (accessed on 15 March 2023).
14. Davis, L.C.; Kress, J.V.; Feldkamp, L.A. Practical cone-beam algortihm. *J. Opt. Soc. Am.* **1984**, *1*, 612–619.

15. Buades, A.; Coll, B.; Morel, J.-M. A Non-Local Algorithm for Image Denoising. In Proceedings of the 2005 IEEE Computer Society Conference on Computer Vision and Pattern Recognition (CVPR'05), San Diego, CA, USA, 20–26 June 2005; IEEE: Piscataway, NJ, USA, 2005; pp. 60–65, ISBN 0-7695-2372-2.
16. Bundesverband der Deutschen Gießerei-Industrie, e.V. BDG. *BDG-Richtlinie P203: Porositätsanalyse Und -Beurteilung Mittels Industrieller Röntgen-Computertomographie (CT)*; Bundesverband der Deutschen Gießerei-Industrie e.V. BDG: Düsseldorf, Germany, 2019.